A large-stroke planar positioning stage for

The growing demand from industry for high-precision systems introduces new challenges for positioning mechanisms. High accuracy and repeatability down to the sub-micron scale are not uncommon. This is often combined with extreme environments, like high UV light sources, electron beams or vacuum. This article focuses on the flexure mechanism for a large-stroke planar XY-positioning system. Applications for such a flexure mechanism can be found in for example lithography, micromachining or microscopy.

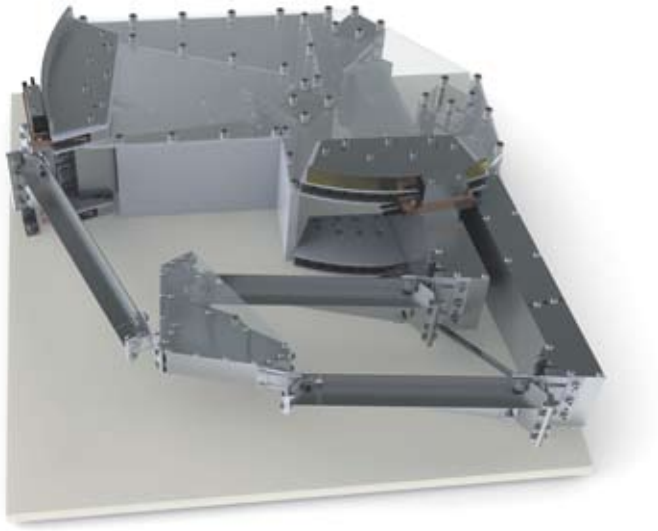

• *Ger Folkersma, Steven Boer, Dannis Brouwer and Just Herder* •

Common large-stroke stages include friction or roller bearings to guide the motion. The friction is normally minimised by applying lubricants. In a vacuum environment however, this lubricant slowly evaporates and will contaminate the vacuum and its surroundings. This will result in excessive wear and increased friction, and reduces the accuracy of the positioning mechanism itself. This can be solved by using solid lubricants for example [1], or by avoiding friction with magnetic or air bearings [2]. However, these methods increase the mechanism complexity considerably.

Flexure elements for guiding the motion do not have this problem, since these elements do not need any lubrication and maintenance. Other advantages of flexure hinges are no backlash, diminished friction and high resolution [3].

Authors' note

Ger Folkersma is a Ph.D. student in the field of micro-assembly for optical systems in the group of Mechanical Automation and Mechatronics at the University of Twente, Enschede, the Netherlands. The work described in this article was part of his Master's thesis at the same university. Steven Boer is a Ph.D. student in the field of multi-body modeling of dynamic systems, also in the group of Mechanical Automation and Mechatronics. Dannis Brouwer is assistant professor in the same group and project manager at DEMCON, based in Oldenzaal, the Netherlands. Just Herder is professor in the same group and associate professor at Delft University of Technology, Delft, the Netherlands.

www.wa.ctw.utwente.nl

2-DoF flexure-based vacuum environments

The mechanism described here combines a large stroke with elastic cross hinges.

Mechanism layout

The specifications for this mechanism state a square workspace of 100 x 100mm^2, and a maximum size for the complete mechanism of 500 x 500 x 85 mm^3. For high-precision applications, the stability of the stage is important, which translates to a minimum natural frequency, with blocked actuators, of 100 Hz. Without actuators, this is the third natural frequency of the mechanism, since the first two modes are the desired X- and Y-motions of the end-effector.

A conceptual layout is shown in Figure 1. First, two parallelograms E-C-G and G-F-D restrict the in-plane rotation of the end-effector. An actuator around hinge 2 defines the end-effector position along the X-axis. Another arm-pair A-B, with an actuator around hinge 1, defines the end-effector position along the Y-axis. This approach allows placement of the actuators at the base, which reduces the negative effect of the weight of the actuator on the third natural frequency.

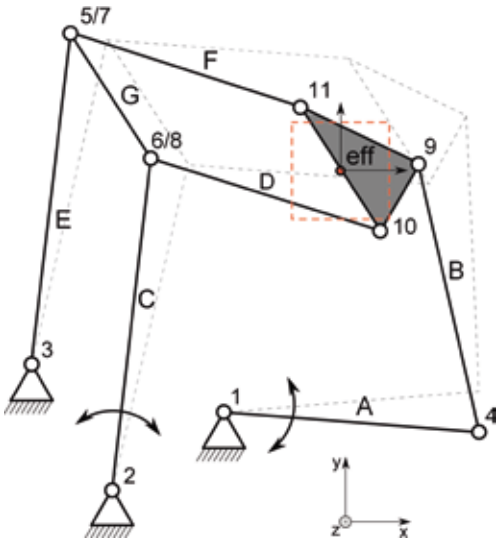

Figure 1. Schematic layout of the mechanism. Elastic hinges are indicated by numbers, connecting arms by letters.

The hinge positions are optimised by an algorithm that minimises the total mechanism size and constrains the rotation of the hinges to be within the material stress limits.

Cross hinges

Cross hinges (also known as cross-spring pivots) consist of multiple-leaf springs mounted perpendicular to each other. Having only one degree of freedom (DoF), this element functions like a regular hinge. The simplest cross hinge consists of two leaf springs; see Figure 2.

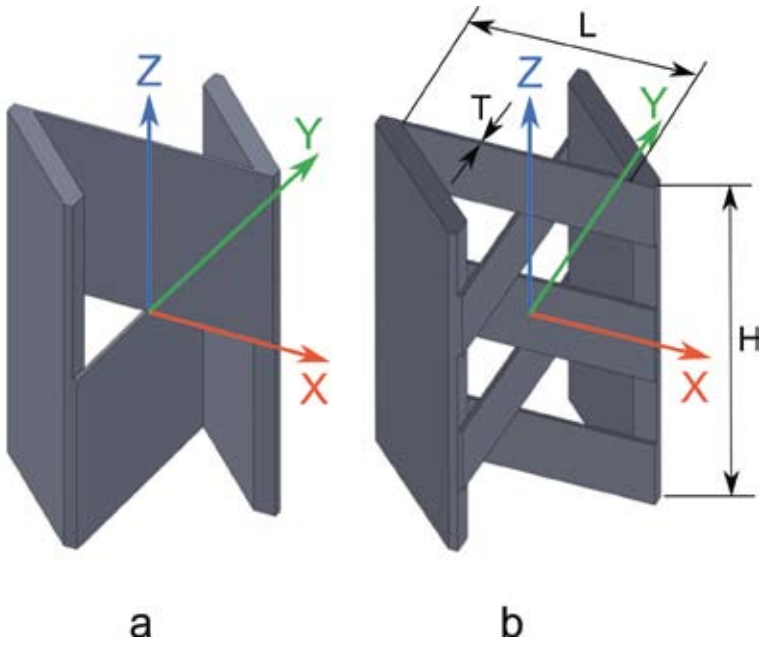

Figure 2. Various configurations of cross-hinges.
(a) 2-leaf.
(b) 5-leaf.

Figure 3 shows the stiffness versus the hinge rotation, for the two variations of a cross hinge. The dimensions of the leaf springs are listed in Table 1. The stiffness is calculated in the geometrical center of the cross hinge, with the directions orientated as indicated in the figure, where for example CRx denotes the rotational stiffness about the x-axis.

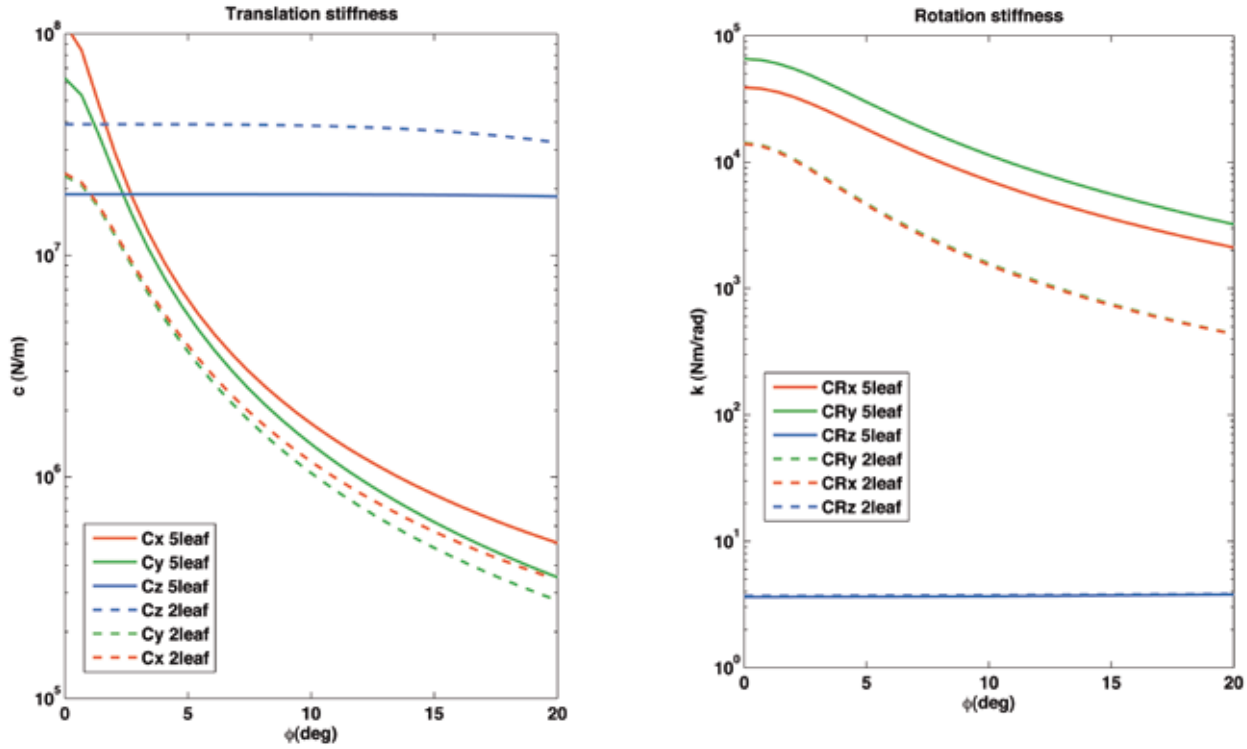

Figure 3. SPACAR simulation of stiffness vs. hinge deflection ϕ, for the two cross-hinge variations.

Table 1. Dimensions of analysed cross-hinges.

Type	*H* (mm)	*L* (mm)	*T* (mm)	leaf spring height (top to bottom) (mm)
2-leaf	85	50	0,5	42; 42
5-leaf	85	50	0,5	15; 10; 33; 10; 15

Ideally, the stiffness is high in all directions except for the desired hinge rotation CRz. This is the case for zero deflection. However, with increasing deflection the stiffness in all directions, except for rotation about the Z-axis and translation along the Z-axis, drops fast. This will result in a lower unwanted natural frequency of the mechanism when it moves outside the nominal position.

To optimise the supporting stiffness, the leaf springs are divided in multiple parts (see Figure 2b). The rotational stiffnesses around the X- and Y-axis are now higher over the full hinge rotation. This comes at the price of losing translational stiffness in the Z-direction. However, since the expected dominant load at the cross hinges is a moment around the X- and Y-axis, this is of low influence. As a result of the nonsymmetrical geometry, the rotational stiffness of the optimised cross hinge is higher around the Y-axis as compared to the X-axis. This difference is taken into account in the mechanism design, by rotating the cross hinges in such a way that the maximum supporting stiffness is in the direction of the maximum expected load.

Mechanism design

The mechanism is designed to be exact constraint, which means that there are no over- or underconstraints in the complete mechanism. Overconstraint mechanisms usually have internal stresses due to manufacturing imperfections or aligning problems. These internal stresses can influence the dynamics of the system [4], resulting in an undeterministic design and loss of supporting stiffness. Underconstraints lead to internal vibration modes at relatively low frequencies. In exact constraint design, the overconstraints are released at pre-defined locations. Therefore misalignment does not lead to large a internal stress. This ensures the mechanism exhibits deterministic behaviour, even when parts are misaligned.

To examine the over- and underconstraints in this mechanism, at first it is assumed that each arm is rigid, and each hinge releases one DoF. Now each pair of upper and lower arms (AB, CD, EF, see Figure 1) with three hinges (1-4-9, 2-6-10, 3-5-11) releases three DoFs: translations in X- and Y-direction, and one rotation about the Z-axis, see Figure 4.

Without arm G, the end-effector therefore has the same three released DoFs. With the X- and Y-translation actuated, the rotation about the Z-axis should be constrained by arm G. This means this arm should only fix one DoF to be exactly constrained.

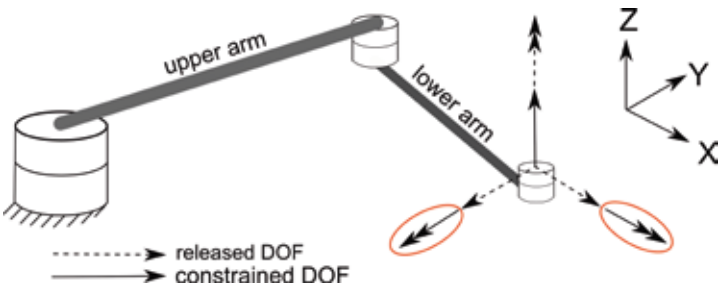

Figure 4. DoFs of one pair of arms (arms assumed rigid).

With three constraints per arm pair, and one from arm G, the end-effector now has $(3 \cdot 3) + 1 = 10$ constrained DoFs, and is therefore overconstrained. Since two DoFs are actuated there are $10 - (6 - 2) = 6$ overconstraints in the mechanism. This means that two DoFs should be released per arm pair. For the arm in Figure 4 these are the encircled DoFs, the rotation about the X- and Y-axis; see Figure 5.

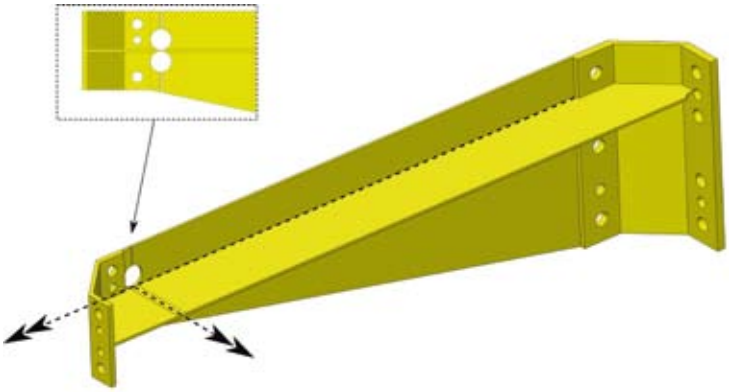

Figure 5. Released DoFs in arm G.

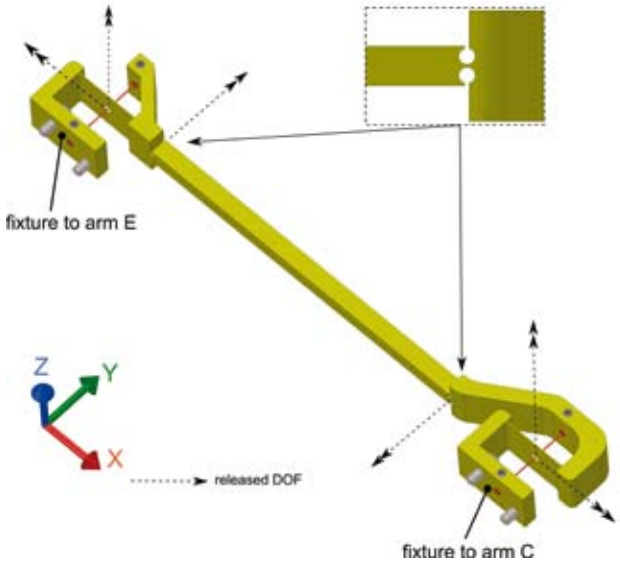

Figure 6. Compliances in lower arms.

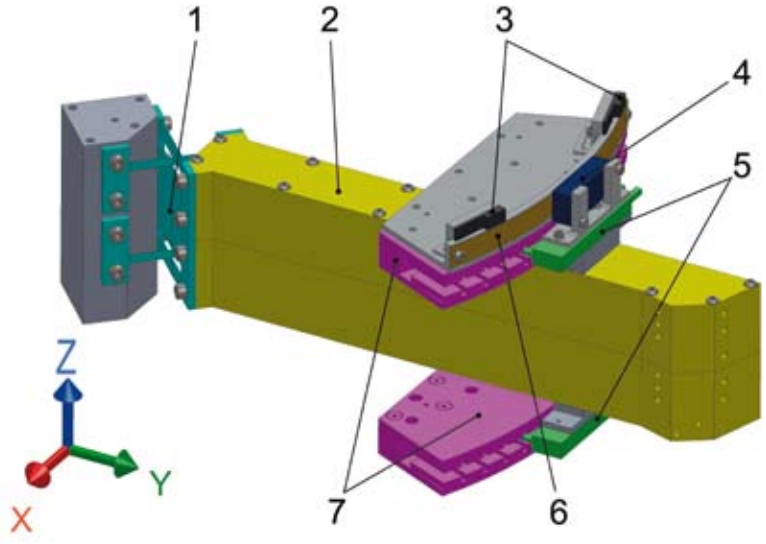

Figure 7. Actuators mounted on an upper arm.
1: Cross hinge
2: Upper arm
3: Limit switch
4: Encoder head
5: Motor coil units
6: Encoder scale
7: Motor magnet yokes

This analysis allows to design the arms to have compliances in the desired directions. Arms A, C and E are supposed to be stiff and lightweight. This can be achieved by creating a closed 'box' structure [5]. The lower arms (B, D, F) connect hinge 4-9, 6-10 and 5-11. As analysed, two compliances need to be added in these arms. It is chosen to create a torsion-compliant beam by creating a T-shaped cross section. The other compliance is added with a notch-flexure at one end; see Figure 6.

Actuation and feedback

As indicated in Figure 1, the mechanism is actuated by rotating arms A and C about hinge 1 and 2, respectively. Actuators that introduce friction or backlash are not suitable, and in order to do experiments with the mechanism a direct-drive actuator is required. This actuator delivers a force in one direction, while small motions in the other directions are possible. This allows for modal measurements on the mechanism, without coupling to the fixed world through the actuators. For this purpose, linear ironless motors are modified to have an arc-shaped trajectory by redesigning the magnet yokes; see Figure 7 #7. The (standard) coil units are fixed to the arm. Per arm two motors are used, which makes sure the force is distributed symmetrically about the length-axis, and prevents an unnecessary torque on the cross hinges; see Figure 7 #1).

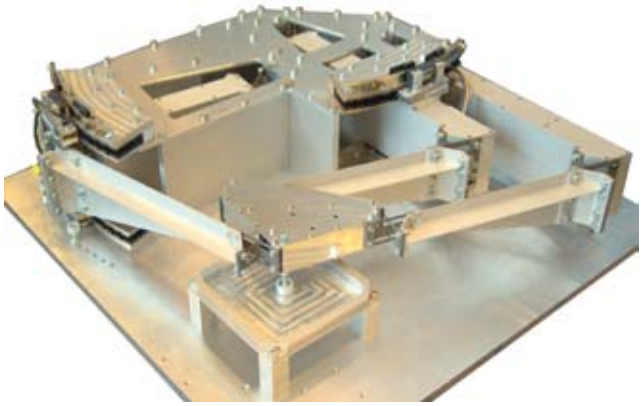

Figure 8. The experimental set-up.

The position of the arm is measured directly at the actuators by optical linear encoders. The steel measuring scale is bent along the same arc as the actuators. This effectively measures the angle of rotation of the cross hinge at the base; see Figure 7 #1. The position of the end-effector is not measured, so a kinematic model from the encoders to the end-effector is used to control its position. Figure 8 shows the experimental set-up.

Characterisation

The first unwanted (third) natural frequency of the mechanism in the central position is determined by FEM analysis (see Figure 9), and is found to be 115 Hz. To verify this, a mechanism identification is carried out. The actuators are supplied with independent pseudo-random binary signals (PRBS), to create excitations in a range between 1 and 500 Hz. A MIMO spectral model and state-space parametric model of order 8 are derived from the in- and output data, using the Matlab Ident toolbox. Figure 10 shows the bode-magnitude plots of both transfer functions. The transfer is between motor force inputs F_x and F_y to encoder outputs Y_x and Y_y. The first two natural frequencies are visible in both models at 1.3 Hz and 2.6 Hz. For higher modes however, the signal-to-noise ratio is low, and no definite conclusion can be drawn for the third natural frequency.

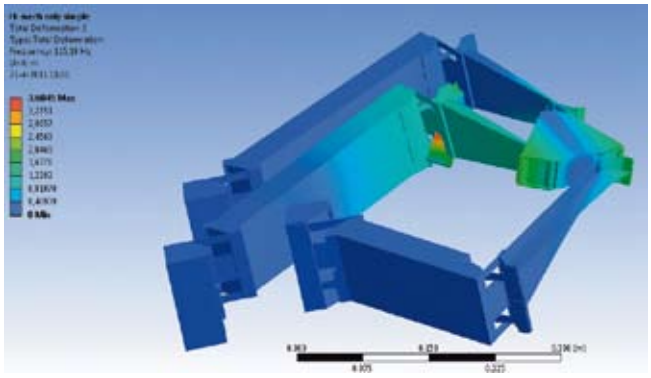

Figure 9. Third mode shape of the mechanism, at 115 Hz.

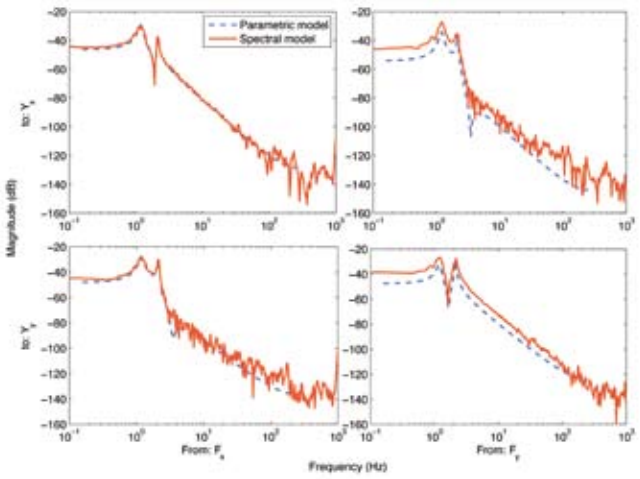

Figure 10. Bode plot of the identification results. With *Yx* and *Yy* the encoder positions, and *Fx* and *Fy* the force supplied to the actuators.

The low signal amplitude is a result of the local motion direction of the vibration. According to the mode shape from the FEM model, the higher modes are mostly vibrating in a direction almost perpendicular to the measurement direction of the encoders and to the actuation direction of the motors. Since the encoders cannot measure the motion of the third mode precisely enough, an additional sensor is needed. An inductive sensor is placed at hinge #9 to measure the relative movement of the end-effector in the Z-direction at this point. Also the actuators cannot excite those modes with enough energy to get a good measurement signal. To get a better signal, the mechanism is excited by means of a simple hammer, striking in the same position and direction as the inductive sensor.

This measurement is repeated in a grid over the workspace of the end-effector. The third natural frequency is plotted for each position in Figure 11. Maximum frequency of this mode is 105 Hz and it is located in the center of the workspace. This result is close to the simulated natural frequencies from Ansys and SPACAR. Outside the center this frequency drops fast, due to the decreasing supporting stiffness of the cross hinges.

Conclusion

In this article the design and evaluation of a 2-DoF elastic stage is discussed. The specification of a third natural frequency higher than 100 Hz has only been met in the central position of the end-effector. Outside this central position, the supporting stiffness of the cross hinges decreases, and therefore the third natural frequency of the mechanism decreases. Ansys FEM and SPACAR models show good agreement on mode shapes and frequencies, but with the current models it is difficult to do accurate modal analysis outside the central position. While this result is not satisfactory according to the specifications, this behaviour

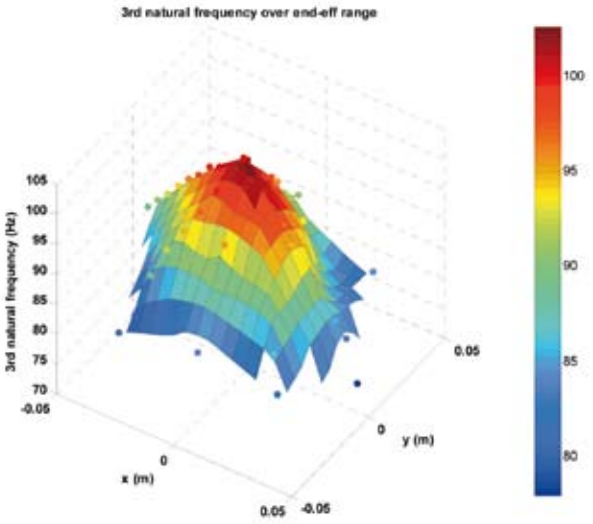

Figure 11. Measured third natural frequency over the workspace.

was expected beforehand and confirms the theory. The results can be used to get a better insight in the behaviour of large deflections in mechanisms. Furthermore, the set-up and measurements can be used to validate future modeling techniques.

To improve the performance of the mechanism, new research has been started to investigate other flexure hinges that have a lower drop in stiffness when rotated.

For more information and some movies of the mechanism, go to http://goo.gl/HUV6i.

References

[1] Nishimura, M. and M. Suzuki, "Solid-lubricated ball bearings for use in a vacuum -- state-of-the-art", *Tribology International*, 1999, Vol. 32(11): p. 637-647.

[2] Sogard, M.R., "Air bearing operable in a vacuum region". 2000, Nikon Corporation.

[3] Hongzhe, Z. and B. Shusheng, "Accuracy characteristics of the generalized cross-spring pivot", *Mechanism and Machine Theory*, 2010, Vol. 45(10): p. 1434-1448.

[4] J. P. Meijaard, D. M. Brouwer, and J.B. Jonker, "Analytical and experimental investigation of a parallel leaf spring guidance", *Multibody System Dynamics*, 2010, Vol. 23(1): p. 77-97.

[5] Soemers, H.M.J.R., Design Principles for precision mechanisms. 2010, Enschede: T-Pointprint.